

Influence of Water/Ethanol Mixing Ratio on Gemcitabine Binding to Cucurbit-7-uril Based on Molecular Dynamics Simulations and Three-Dimensional Reference Interaction Site Model

Natthiti Chiangraeng, Norio Yoshida,* Haruyuki Nakano, Apinpus Rujiwatra, and Piyarat Nimmanpipug*



Cite This: *J. Chem. Inf. Model.* 2025, 65, 4137–4147



Read Online

ACCESS |



Metrics & More

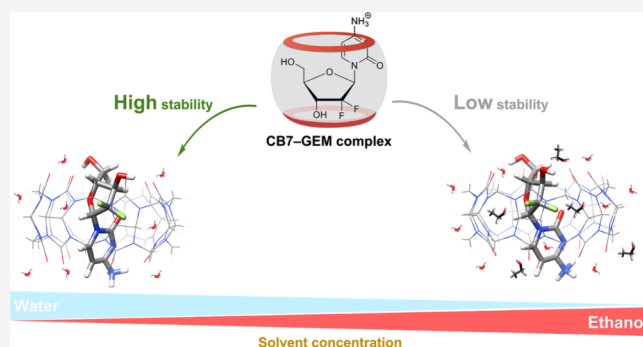


Article Recommendations



Supporting Information

ABSTRACT: Accurate binding affinities of the cucurbit-7-uril–gemcitabine (CB7–GEM) complex in pure water and ethanol/water-mixed solvents were obtained by combining molecular dynamics simulations and three-dimensional reference interaction site model (3D-RISM) calculations. Point charges of CB7 and GEM molecules, depending on solvent mixture ratios, were determined using 3D-RISM self-consistent field (3D-RISM-SCF) calculations. The calculated binding affinities reveal that the most preferable CB7–GEM complex forms in the pure water system. The complexes in the mixed solvents show lower stability at higher ethanol ratios. Stable conformations at different solvent concentrations appear to be a key factor in the obtained trend of binding affinity enhancement. Conformations in the high-water fractions, associated with higher complex stability, exhibit lower internal energies than those in high-methanol fractions. Disruption of hydrogen-bonding formation also plays a crucial role in the solvation free energies. An explicit solvent model is crucial for accurate calculations of CB7–GEM complexes in these binary mixtures, providing results comparable to the experiments.



1. INTRODUCTION

Cucurbit- $[n]$ -urils (CB n) are synthetic macrocycles with carbonyl-rich portals possessing hydrophilic entrances and hydrophobic cavities that can encapsulate suitable drug molecules. These molecules have played a significant role in supramolecular chemistry.^{1,2} Since their discovery, the CB series have received significant interest in their use as a host for various guest molecules through noncovalent bonding interactions. Neutral or positively charged guests tend to bind with CBs with high binding affinity due to ion–dipole interactions between the carbonyl oxygens and guest molecules.¹ A variety of CB types, such as CB5, CB6, CB7, and so forth, have been reported, differing in the number of glycoluril units (n) in their structures.¹ While structurally similar, these CBs exhibit differences in their physical and chemical properties and, consequently, their applications.^{1,3} Among various types of CBs, the CB7, comprising 14 carbonyl groups around both portals, has received considerable attention due to its outstanding water solubility and biocompatibility.^{1,4,5} The properties of CB7, therefore, make it promising molecular containers for drug molecules, as evidenced by previous research.^{1,6–10}

CB7 has been used as a host for various anticancer drugs, including 2-[[5-(4-pyridinyl)-4H-1,2,4-triazol-3-yl]thio]acetic acid,⁶ oxaliplatin,⁷ platinum(II)-based drugs,^{8,9} mitoxantrone,¹⁰ and gemcitabine.^{11,12} Among these, gemcitabine (GEM) or 2'-

deoxy-2',2'-difluorocytidine, has attracted considerable attention in recent years.^{13,14} GEM is used to treat various solid tumors, including lung,^{15,16} breast,¹⁴ pancreatic cancer,^{13,17} and urothelial cancers.¹⁸ Extensive research has aimed to improve GEM and its derivative efficiency in cancer treatments.¹⁹ However, GEM cannot directly diffuse through the human cell membrane without help from the transporters.^{5,11} Developing drug carriers offers a solution to overcome the problems associated with using GEM as anticancer drugs.^{7,8,13,17,20–24} This approach can reduce GEM's toxicity and enhance its efficiency^{7,24} by extending its circulation time.^{7,20} The resulting drug complex can penetrate the human cell membrane.²⁵ Moreover, ethanol has been reported to influence the stability of the CB7–GEM complex. This effect may not only destabilize the complex but also induce adverse effects in the patient.²⁶ Therefore, understanding the influence of ethanol on CB7–

Received: February 6, 2025

Revised: March 31, 2025

Accepted: March 31, 2025

Published: April 10, 2025



GEM complex stability is crucial for its potential use in chemotherapy.

Buczowski et al. revealed the spontaneous formation of the CB7–GEM complex in the aqueous solution.¹² Their analysis showed a 1:1 stoichiometry between CB7 and GEM. They also reported that the CB7–GEM complexes can be affected by pH, sodium chloride concentration, and the presence of ethanol.^{11,27} Low pH can promote the protonation of GEM, which interacts favorably with negatively polarized carbonyl groups surrounding the CB7 portal, resulting in increased binding affinity.²⁷ However, the presence of ethanol destabilizes the complex, leading to a decrease in binding affinity.¹¹ Recently, Venkataramanan and co-workers studied CB–GEM complexes using density functional theory (DFT) calculations.²⁸ Their results showed that the CB7–GEM complex exhibited the greatest binding free energy in the solution phase using the implicit solvent models compared to CB6–GEM and CB8–GEM complexes. The CB7–GEM complex has the highest binding affinity, as indicated by a binding energy of $-19.13 \text{ kcal}\cdot\text{mol}^{-1}$, compared to $-15.25 \text{ kcal}\cdot\text{mol}^{-1}$ for CB8–GEM and $-2.91 \text{ kcal}\cdot\text{mol}^{-1}$ for CB6–GEM. Further investigation of the interactions between CBs and GEM molecules is needed to fully clarify the effect of this binary solvent system on the complex stability.

The combined use of molecular dynamics (MD) simulations and the three-dimensional reference interaction site model (3D-RISM) calculations has proven valuable in studying various host–guest complex systems, yielding results comparable to experimental data.^{3,29} MD simulations are suitable for simulating complexes in solution and generating representative structures for further analysis. At the same time, the 3D-RISM calculation is a better choice for the calculation of solvation free energy. Combining the advantages of these approaches leads to accurate binding affinity. The 3D-RISM theory is based on statistical mechanics derived from the molecular Ornstein–Zernike equation.³⁰ This theory is suggested for calculating solvation properties because it explicitly accounts for solute–solvent and solvent–solvent interactions through pairwise intramolecular interactions, and the configurational integral over solvent molecules is calculated analytically.³¹ Furthermore, this method allows the calculation of the solvent reorganization energies.^{3,29} These reorganization properties are essential for investigating solute–solvent interactions and can facilitate the determination of the system's partial molar volume.³² These methods have demonstrated accurate binding affinity predictions for CB-guest complexes in aqueous solution compared with the experimental results.²⁹

Based on previous studies, we will investigate the inclusion complex between CB7 and GEM using computational approaches, especially MD simulations and 3D-RISM calculations. CB7 will serve as the host, and protonated gemcitabine (GEM) will be the guest molecule, denoted as “GEM” throughout this work. The chemical structures of CB7 and GEM are shown in Figure 1. In our study, we will simulate CB7–GEM complexes in pure water solvent and water/ethanol (EtOH) mixtures with ethanol weight fractions of 0, 1, 2, 5, 10, and 15%w/w based on the experimental report.¹¹ The effect of solvent concentration on the complex structures and the binding affinity will be investigated. Given the limited experimental and extremely scarce theoretical studies on the CB7–GEM complex, our findings will contribute to its design for drug delivery applications. We also anticipate that these proposed computational methods can serve as a reference model for studying other host–guest complexes in binary solvent systems.

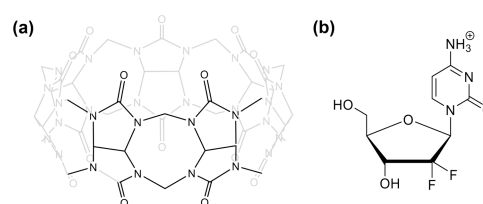


Figure 1. Chemical structures of cucurbit-7-uril (CB7) and gemcitabine (GEM).

2. COMPUTATIONAL DETAILS

2.1. Preparation of Structures and Partial Charge Evaluation. Point charges of each atom for CB7 and GEM molecules were estimated using the three-dimensional reference interaction site model self-consistent field (3D-RISM-SCF) method, which incorporates *ab initio* molecular orbital.^{33–36} This method was implemented in the general atomic and molecular electronic structure system (GAMESS) program (version 18 August 2016).³⁷ In these 3D-RISM-SCF calculations, the number density and dielectric constant, corresponding to the ethanol/water weight fractions, were used. The dielectric-consistent RISM theory was used to obtain the solvent susceptibility.³⁸ Number density values were directly calculated from solution densities obtained experimentally,³⁹ while solution dielectric constants were obtained from the Gaussian 16 library.⁴⁰ These crucial parameters are summarized in Table 1. The LJ parameters from the general AMBER force field

Table 1. Dielectric Constant, Solution Density, and the Number Density of Ethanol and Water in Each Percentage of Ethanol Weight Fraction

| percentage of ethanol weight fraction | dielectric constant | solution density (g/cm ³) | number density (molecule/Å ³) | |
|---------------------------------------|---------------------|---------------------------------------|---|--------------|
| | | | ethanol | water |
| 0 | 78.40 | 0.99708 | | 0.0333390769 |
| 1 | 78.14 | 0.99520 | 0.0001301692 | 0.0329434537 |
| 2 | 77.93 | 0.99336 | 0.0002598571 | 0.0325503984 |
| 5 | 77.28 | 0.98817 | 0.0006462487 | 0.0313890980 |
| 10 | 76.13 | 0.98043 | 0.0012823737 | 0.0295041200 |
| 15 | 74.90 | 0.97334 | 0.0019096502 | 0.0276634959 |

(GAFF) were used. The target molecules were calculated using the B3LYP functional at 298.0 K. The Kovalenko–Hirata (KH) closure was used.^{30,41} The point charges of each atom were calculated using an explicit solvent model.

2.2. Molecular Dynamics (MD) Simulations. All MD simulations were performed using AMBER20 software.⁴² Potential parameters for CB7 and GEM were taken from the GAFF library, consistent with the 3D-RISM-SCF calculations. The point charges of both molecules were obtained from the 3D-RISM-SCF calculations. Initial structures in each weight fraction were generated using the PACKMOL code.⁴³ The tleap module was then used to assign potential parameters to the PACKMOL generated structures, creating the topology and coordinate files required for the AMBER program. Explicit water solvation was modeled using the TIP3P model. The initial ethanol structure was prepared using Gaussian 16 software.⁴⁰ The ethanol molecule was optimized using DFT at the B3LYP/6–31G level in vacuum and subsequently converted the Gaussian output file to a tleap input file using the Antechamber tool.⁴² In this study, the number of water molecules was kept

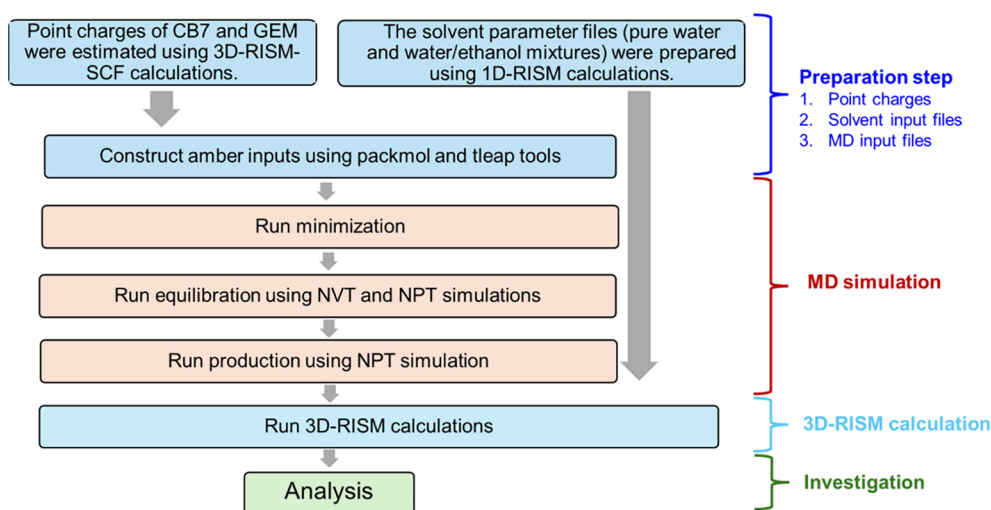


Figure 2. Scheme of the overview simulation procedure.

constant at 1000 molecules, while the number of ethanol molecules was varied to match the reported experimental concentration.¹¹

All systems were simulated using the same protocol (Figure 2). Energy minimization was performed for 10,000 cycles using the PMEMD.CUDA in explicit solvent.^{44–46} The steepest descent was used for the initial 2,500 steps, followed by the conjugate gradient method for the remaining cycles. Subsequently, the system equilibrated using 125 ps canonical ensemble (NVT) and 0.5 ns the isothermal–isobaric ensemble (NPT) simulations. Temperature was controlled using the Langevin dynamics, and the SHAKE algorithm was used to constrain all hydrogen atoms.⁴⁷ The production NPT simulations were performed for 100 ns. All simulations were conducted at a temperature of 298.0 K and a pressure of 1 atm.

2.3. Analysis of Structural Properties. Prior to 3D-RISM calculations, the stability of the simulated complex was assessed by analyzing the root-mean-square deviation (RMSD) of atomistic positions from the MD trajectory using the CPPTRAJ module.⁴⁸ This analysis allows for the evaluation of structural changes during the simulation. Subsequently, 1,000 frames at equilibrium will be sampled for further analysis and used as the initial structures for 3D-RISM calculations.

2.4. 3D-RISM Calculations. All 3D-RISM calculations were conducted using the reference interaction site model integrated calculator (RISMicCal) package.^{49,50} The structures of the CB7 and GEM molecules within the complex, obtained from the MD simulations without solvent molecules, were treated as solute molecules in the 3D-RISM calculations. Water and ethanol molecules, as solvent were regenerated by 3D-RISM code according to the weight fractions listed in Table 1. In this study, the solute molecules were assumed to be infinite dilution. The KH closure was chosen due to the excellent convergence.^{41,51,52} 3D-RISM was performed on a grid of 128³ points and a grid spacing of 0.5 Å.

2.5. Analysis of Energetic Properties. Internal interaction and solvation free energies were calculated from MD simulations and 3D-RISM calculations, respectively. The internal interaction energy was calculated from the MD trajectory using the CPPTRAJ module,⁴⁸ while the solvation free energy was directly obtained from the 3D-RISM output files.

3. RESULTS AND DISCUSSION

3.1. Variation of Point Charges of CB7 and GEM in the Different Solvents. Prior to the MD simulation and the 3D-RISM calculation, the point charges for each atom of CB7 and GEM molecules must be determined depending on the solvent environments. In this work, the point charges were calculated using the 3D-RISM-SCF method for CB7 and GEM in binary solvent systems, as shown in Figure 3 and Figure S1,

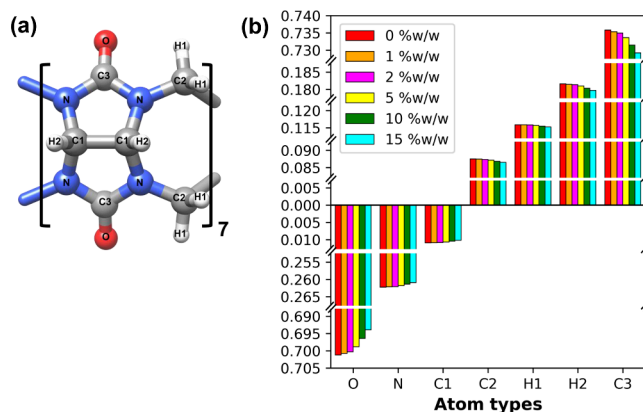


Figure 3. (a) Labeled atom types in the CB7 structure and (b) calculated point charges of each atom type at each weight fraction of ethanol from 0 to 15%w/w.

respectively. In the case of the CB7 molecule, the point charge of atoms generally increases as the weight fraction of ethanol decreases from 15 to 0%w/w. This suggests a slight decrease in the overall polarization of the CB7 molecule in a higher ethanol content system, corresponding to a weakening of the electrostatic interactions between the solute and solvent, as ethanol has lower polarity compared to water. On the other hand, as shown in Figure S1, there is no significant difference in point charges of the GEM molecule by changing the solvent fraction.

3.2. Structural Changes of CB7 and GEM in Pure and Mixed Solvents. RMSD analysis was performed to assess the complex binding features and stability in different solvent environments before selecting structures for further analysis and calculations. RMSD profiles of CB7, GEM, and the CB7–GEM complex were analyzed from MD trajectories as shown in Figure

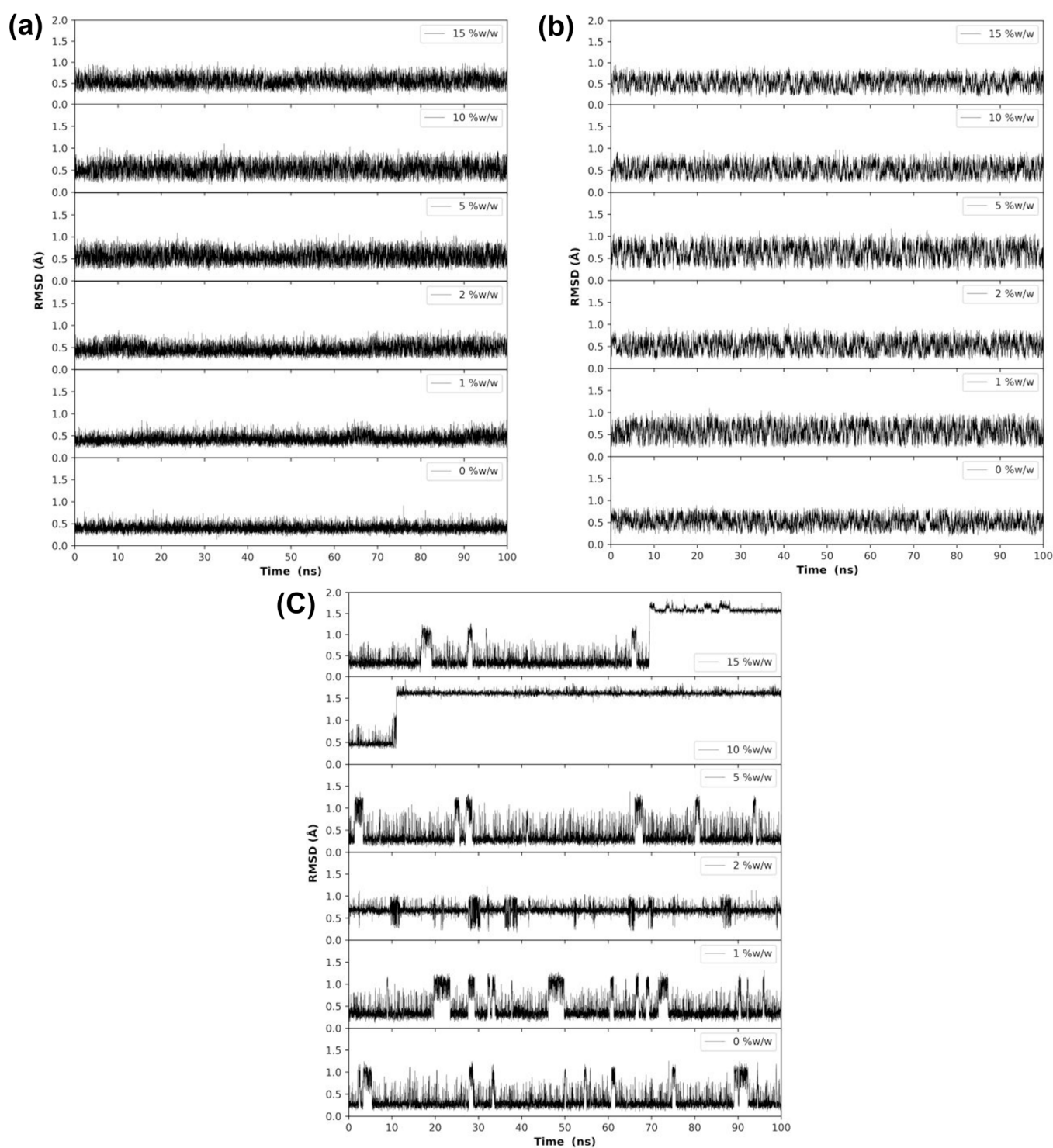


Figure 4. RMSD profiles of (a) CB7, (b) CB7–GEM complexes, and (c) GEM in each weight fraction of ethanol.

4. In the cases of CB7 and CB7–GEM complex, the structures remained stable throughout the simulation period in all binary solvent systems. However, for the GEM system, the RMSD profiles in 10 and 15%w/w ethanol exhibit a discontinuity, indicating a conformational change as shown in Figure 4c. The representative structures of both stages are shown in Figure 5. Analysis of the structures revealed that the hydroxy group of the GEM side chain undergoes conformational change in the presence of 0%–5%w/w ethanol. In contrast, at higher ethanol concentrations (10%w/w and 15%w/w), the rotation of the

pyrimidine membered ring was indicated. These structural changes resulted in the change of RMSD, as shown in Figure 4c.

3.3. Binding Free Energy of CB7–GEM Complexes.

This work presents a systematic investigation of the CB7–GEM complexes in ethanol–water mixtures were conducted. The binding free energy ΔG_{bind} of a CB7–GEM complex system can be defined as follows:

$$\Delta G_{\text{bind}} = \Delta E_{\text{mm}} + \Delta G_{\text{solv}} \quad (1)$$

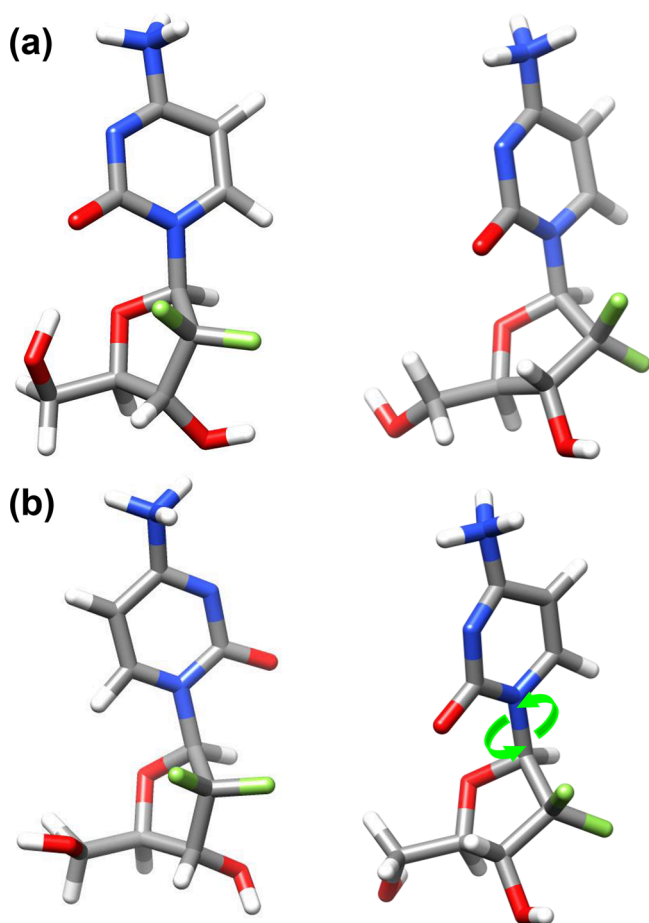


Figure 5. GEM structures at (a) 2%w/w and (b) 15%w/w ethanol. Left panel: GEM structure obtained from the simulations of the isolated molecule. Right panel: GEM structure obtained from simulations of the CB7–GEM complex.

where the internal interaction energy (ΔE_{mm}) and solvation free energy (ΔG_{solv}), obtained from MD simulations and 3D-RISM methods, respectively. Figure 6 illustrates ΔG_{bind} and its components (ΔE_{mm} and ΔG_{solv}). The left panel of Figure 6 shows absolute values obtained from simulations, while the right panel depicts the relative values for comparison. From Figure 6, ΔG_{bind} systematically increases with increasing ethanol concentration in the solution, indicating a decrease in the stability of GEM within the CB7 cavity. This observation is consistent with experimental findings.¹¹ Binding affinities obtained from experiment and from this work are compared in Figure 7. Our computational results overestimate the magnitude of the binding free energy by approximately 6 kcal·mol⁻¹ compared to experimental values across all ethanol fractions. However, the trend in response to changes in the ethanol fraction is reproduced almost quantitatively.

In comparison to other studies, Venkataraman and co-workers reported a calculated Gibbs free energy of binding of -19.13 kcal·mol⁻¹ for the CB7–GEM complex in the solution phase using DFT calculations with an implicit solvent model.²⁸ In our study, the calculated binding free energy was -12.48 kcal·mol⁻¹, which is closer to the experiment value of -5.71 kcal·mol⁻¹.¹¹ This improvement in the calculated values is attributed to the explicit treatment of atomic-level interactions between solvent molecules. Notably, the trend of ΔG_{bind} with increasing ethanol content is the same as that of ΔE_{mm} , while the ΔG_{solv}

provides the opposite trend, decreasing with increasing ethanol content. As explained in the methodology, the explicit solvent model was used consistently throughout the study, including in point charge estimation, MD simulations, and 3D-RISM calculations. These realistic models yield calculated binding affinities that are more consistent with experimental observations.

3.4. Contributions of Energy Components to the Binding. The contributions of components of ΔE_{mm} were analyzed to give insightful details on energy components dominating CB7–GEM binding affinity. The ΔE_{mm} is composed of three components regarding the CB7–GEM interaction energy $\Delta E_{\text{mm}}^{\text{interaction}}$, and structural energy changes because of the binding between CB7 and GEM molecules that are denoted as $\Delta E_{\text{mm}}^{\text{GEM}}$ and $\Delta E_{\text{mm}}^{\text{CB7}}$, respectively, as follows:

$$\Delta E_{\text{mm}} = \Delta E_{\text{mm}}^{\text{interaction}} + \Delta E_{\text{mm}}^{\text{GEM}} + \Delta E_{\text{mm}}^{\text{CB7}} \quad (2)$$

The calculated $\Delta E_{\text{mm}}^{\text{interaction}}$, $\Delta E_{\text{mm}}^{\text{GEM}}$, and $\Delta E_{\text{mm}}^{\text{CB7}}$ are shown in Figure 8. In this case, no trend was observed for $\Delta E_{\text{mm}}^{\text{interaction}}$. Based on $\Delta E_{\text{mm}}^{\text{GEM}}$, the complex structures can be classified into two groups. The first group has lower energy, consisting of 0 to 5%w/w, whereas the second group has higher energy (10 and 15%w/w). In the first group, we found that the small change in energy between the GEM structure from the isolate simulation and the GEM structure in the complex is due to the hydroxy group in the side chain during the simulation, as shown in Figure 5a. The representative GEM structures from the isolated simulation and the CB7–GEM complex are depicted on the left- and right-hand sides, respectively. In the second group, the large change in energies came from the rotation of the pyrimidine-membered ring in the GEM molecule (see Figure 5b). This rotation requires more energy to rearrange the structure and the difference in the structures between isolated simulation and from the CB7–GEM complex, resulting in large energy differences, as demonstrated in Figure 8b. The $\Delta E_{\text{mm}}^{\text{CB7}}$ values can be explained in the same manner. Small energy changes occur at 0 and 1%w/w, with large energy charges occurring in the remaining systems. The structural difference between isolate simulation and CB7 structure from the complex governed these energy changes. The representative structures are shown in Figure S2.

The contributions of components of ΔG_{solv} was also analyzed. These include four contributions,⁵³ as follows:

$$\Delta G_{\text{solv}} = \Delta E_{\text{interaction}}^{\text{uv}} + \Delta E_{\text{reorg}}^{\text{vv}} - T\Delta\Delta S + \Delta E_{\text{correction}} \quad (3)$$

The $\Delta E_{\text{interaction}}^{\text{uv}}$, $\Delta E_{\text{reorg}}^{\text{vv}} - T\Delta\Delta S$, and $\Delta E_{\text{correction}}$ are solute–solvent interaction energy, solvent reorganization energy, solvation entropy change, and energy correction term, respectively. The $\Delta E_{\text{correction}}$ is calculated based on the pressure correction method^{54,55} as

$$\Delta E_{\text{correction}} = -P(\Delta V^{\text{CB7-GEM}} - (\Delta V^{\text{CB7}} + \Delta V^{\text{GEM}})) \quad (4)$$

where P and ΔV are the system pressure and the partial molar volume (obtained from 3D-RISM calculations), respectively. All components of ΔG_{solv} are shown in Figure 9. The major contributions for ΔG_{solv} came from $\Delta E_{\text{interaction}}^{\text{uv}}$ and $\Delta E_{\text{reorg}}^{\text{vv}}$, while the $-T\Delta\Delta S$ and $\Delta E_{\text{correction}}$ are minor contributions. In Figure 9a, the $\Delta E_{\text{interaction}}^{\text{uv}}$ values decrease with increasing

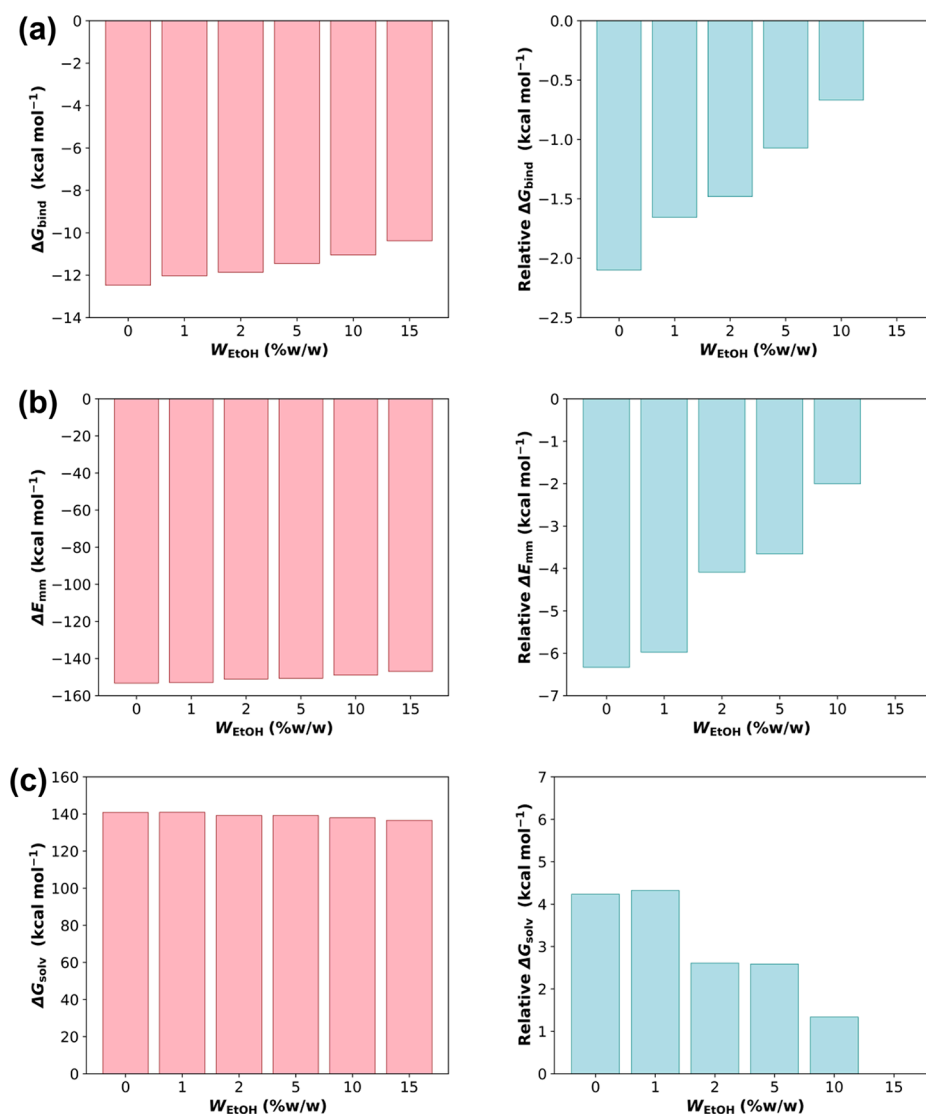


Figure 6. Binding free energy and its components shown on the left-hand side: (a) binding free energy ΔG_{bind} , (b) internal interaction energy change ΔE_{mm} , and (c) solvation free energy change ΔG_{solv} . The relative values of binding free energy and its components, determined by the difference from the minimum of each component, are shown on the right-hand side of each panel.

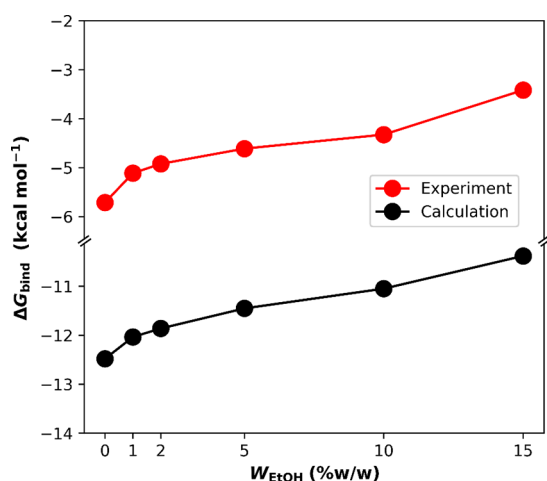


Figure 7. Binding free energy from the experiment (red line)¹¹ and calculation in this work (black line).

ethanol content, while $\Delta E_{\text{reorg}}^{\text{vv}}$ exhibit the opposite trend. Solvation structures from the 3D-RISM calculation indicate that the ethanol and water are well-mixed in the mixture (Figure S3). The decrease in $\Delta E_{\text{interaction}}^{\text{uv}}$ (Figure 9a) with added ethanol is likely due to the loss of hydrogen-bonding (H-bonding) between CB7 or GEM solute molecules and water solvent molecules. Higher ethanol ratios weaken the formation of strong H-bonding between water molecules compared with the pure water solvent. Consequently, the energy penalty decreases at higher ethanol content due to the weakening of the water H-bonds, facilitating solvent displacement from the CB7 cavity upon complex formation. However, the reorganization energy $\Delta E_{\text{reorg}}^{\text{vv}}$ (Figure 9b) is relatively low in the water-rich systems because the displaced solvents can form stronger H-bonds outside the CB7 host, releasing more energy compared to the mixtures. Figure 10 depicts the formation of the H-bonding of oxygen and hydrogen atoms of water and ethanol solvent molecules outside the complexes. In the case of pure water solvent (Figure 10a), only the oxygen and hydrogen of water can form the H-bonds, which are strong and contribute significantly

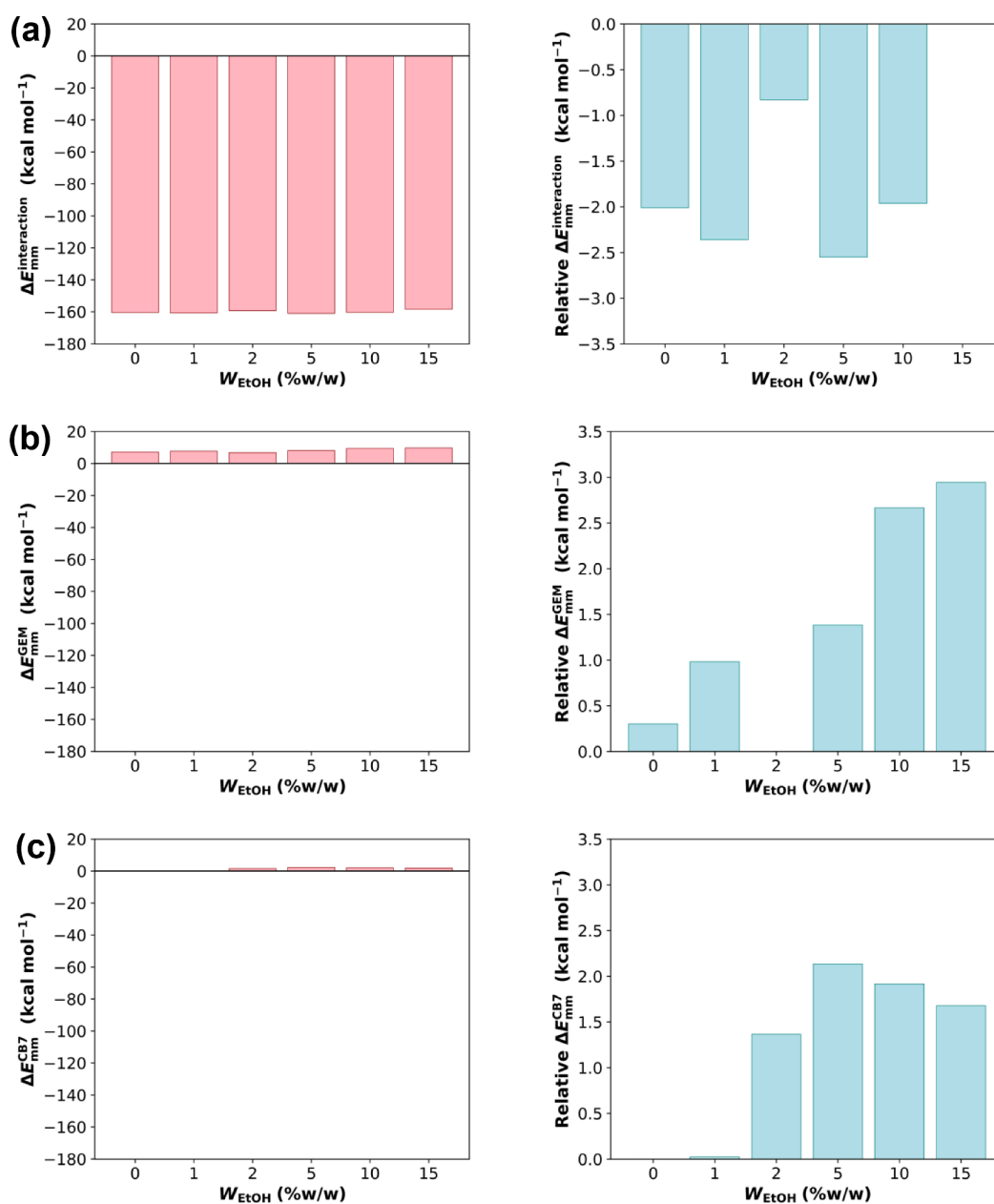


Figure 8. Components of ΔE_{mm} . (a) CB7–GEM interaction energy or $\Delta E_{\text{mm}}^{\text{interaction}}$ and structural energy changes upon binding (b) GEM or $\Delta E_{\text{mm}}^{\text{GEM}}$ and (c) CB7 or $\Delta E_{\text{mm}}^{\text{CB7}}$. Relative values of components of ΔE_{mm} determined by the difference from the minimum of each component are shown on the right-hand side of each panel.

to the solvent reorganization energy component. In contrast, in the mixed solvent, water and ethanol can form weaker hydrogen bonds (Figure 10b,c). Compared to the pure water system, the formation of H-bonds among water molecules (Figure 10a,b) exhibits a similar distribution profile. However, the isosurface plot of three-dimensional distribution functions (3D-DFs) of oxygen and hydrogen in ethanol (Figure 10c) indicated that water–ethanol and ethanol–ethanol interactions occur at the same interacting positions near the hydrophilic entrances. The presence of ethanol can weaken H-bonds compared to the pure water solvent, resulting in higher reorganization energy.

4. CONCLUSIONS

MD simulations and 3D-RISM calculations were carried out to investigate the binding affinity of CB7–GEM complexes in

various binary solvents of ethanol and water. Prior to these computations, the point charges of the constituent atoms of CB7 and GEM were calculated using the 3D-RISM-SCF method at the actual concentrations of ethanol and water, resulting in accurate point charges for use in the MD simulations and 3D-RISM calculations in the mixtures. We found that the calculated binding affinity decreases with increasing ethanol content. Our analysis results suggest that the main factors governing this trend are structural changes and the disruption of H-bonding between the complex and the solvent. Our findings are also qualitatively consistent with the experimental results. In the mixed solvent system, we found that simulations using the explicit solvent model can provide accurate binding affinities. The more precise values are obtained by properly accounting for all molecules in the system, including solute molecules, such as CB7 and GEM,

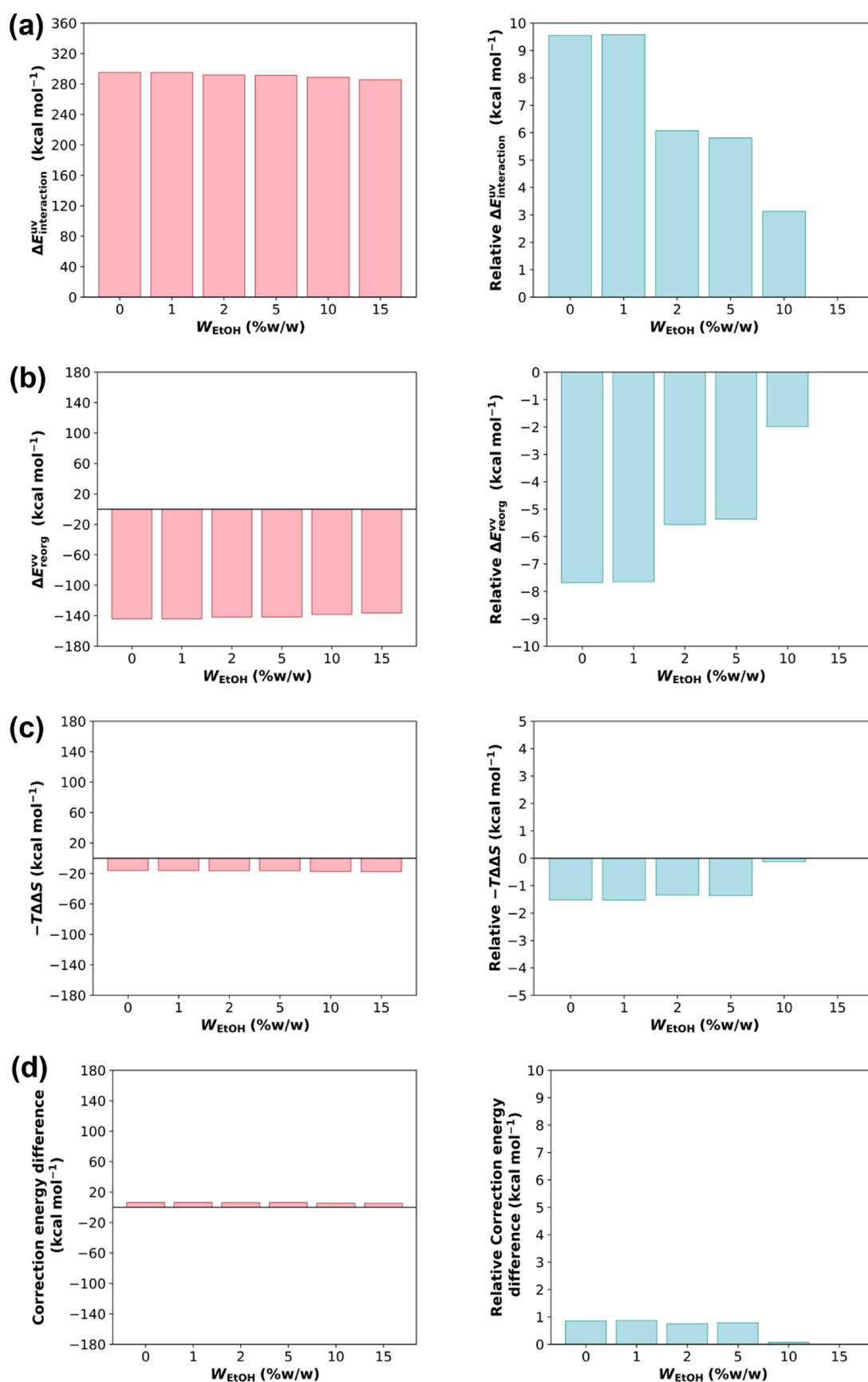


Figure 9. Components of ΔG_{solv} shown on the left-hand side: (a) solute–solvent interaction energy $\Delta E_{\text{interaction}}^{\text{uv}}$, (b) solvent reorganization energy $\Delta E_{\text{reorg}}^{\text{vv}}$, (c) solvation entropy change $-T\Delta\Delta S$, and (d) energy correction term $\Delta E_{\text{correction}}$. Relative values of components of ΔG_{solv} determined by the difference from the minimum of each component are shown on the right-hand side of each panel.

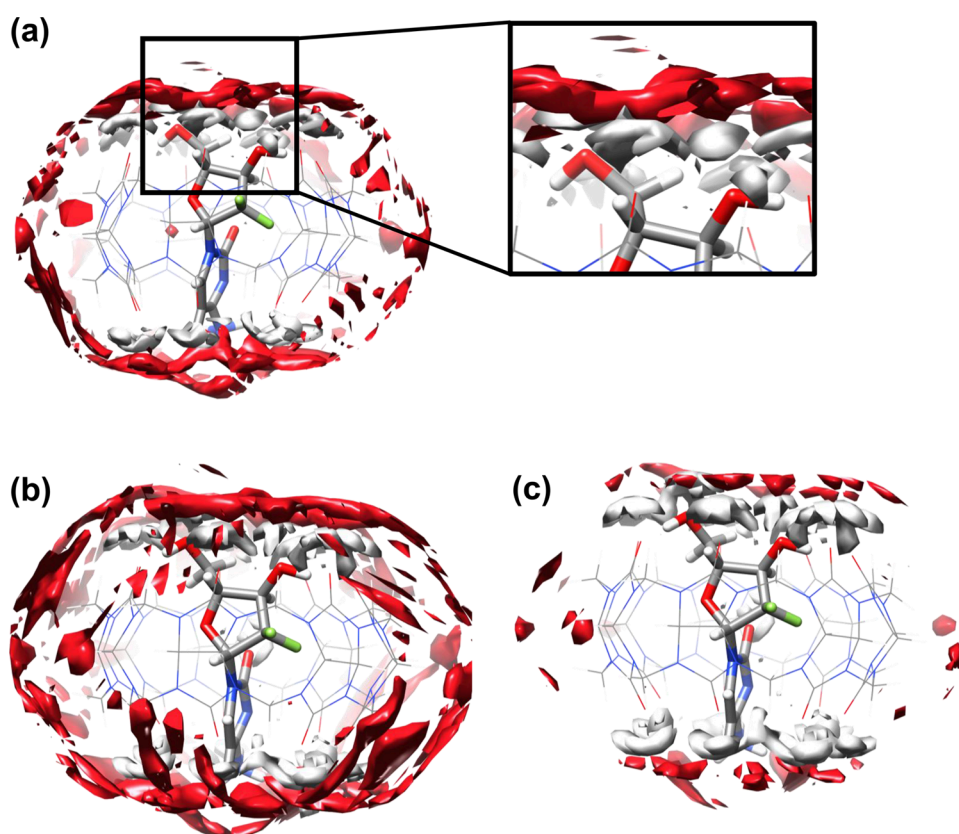


Figure 10. Solvation structure of CB7–GEM complexes at (a) 0%w/w and (b, c) 15%w/w. Panels (a) and (b, c) represent the water-rich and ethanol-rich systems, respectively. Isosurfaces of oxygen ($g_{\text{O}}(r) = 3.0$) and hydrogen ($g_{\text{H}}(r) = 3.0$) are depicted in red and gray colors, respectively. Panels (a) and (b) show the isosurfaces of oxygen and hydrogen of the water solvent, while the panel (c) depicts the isosurfaces of oxygen and hydrogen of the ethanol solvent. In the case of ethanol, the isosurfaces of the rest of the ethanol segments (CH_3- and CH_2-) are omitted for clarity. The zoom-in figure illustrates the formation of an H-bonding of water outside the CB7–GEM complex as an example.

and solvent molecules using the explicit model with fewer approximations.

■ ASSOCIATED CONTENT

Data Availability Statement

RISMical is available in a public repository on GitHub (<https://github.com/rismical-dev/rismical>); PACKMOL used in this work is openly available at <https://github.com/m3g/packmol>. The software and input parameters used in this study have been elaborated in the [Computational Details](#) section. The atomic coordinates for MD simulations, along with point charges from 3D-RISM-SCF calculations of CB7 and GEM in this study, are available in the [Supporting Information](#).

SI Supporting Information

The Supporting Information is available free of charge at <https://pubs.acs.org/doi/10.1021/acs.jcim.5c00225>.

Calculated point charges of GEM structure at various weight fractions, structures of the CB7 obtained from the isolated and complex simulations in 0 and 5%w/w of ethanol, solvation structures of CB7 in different mixed solvents, and atomic coordinates and point charges obtained from the 3D-RISM-SCF calculations for CB7 and GEM ([PDF](#))

■ AUTHOR INFORMATION

Corresponding Authors

Norio Yoshida – Department of Complex Systems Science, Graduate School of Informatics, Nagoya University, Nagoya 464-8601, Japan; orcid.org/0000-0002-2023-7254; Email: noriwo@nagoya-u.jp

Piyarat Nimmanpipug – Department of Chemistry, Faculty of Science, Chiang Mai University, Chiang Mai 50200, Thailand; orcid.org/0000-0001-6364-504X; Email: piyarat.n@cmu.ac.th

Authors

Natthiti Chiangraeng – Department of Chemistry, Faculty of Science and Office of Research Administration, Chiang Mai University, Chiang Mai 50200, Thailand; orcid.org/0000-0002-6141-7067

Haruyuki Nakano – Department of Chemistry, Graduate School of Science, Kyushu University, Fukuoka 819-0395, Japan

Apinpus Rujiwatra – Department of Chemistry, Faculty of Science, Chiang Mai University, Chiang Mai 50200, Thailand; orcid.org/0000-0002-2364-4592

Complete contact information is available at <https://pubs.acs.org/doi/10.1021/acs.jcim.5c00225>

Author Contributions

N.C. performed conceptualization, methodology, formal analysis, investigation, visualization, and writing—original draft. N.Y.

performed conceptualization, supervision, writing—review & editing, funding acquisition, resource gathering, and software. H.N. performed writing—review & editing, resource gathering, and software. A.R. performed supervision, writing—review & editing, and funding acquisition. P.N. performed conceptualization, supervision, writing—review & editing, funding acquisition, and resource gathering.

Notes

The authors declare no competing financial interest.

ACKNOWLEDGMENTS

This research was supported by Chiang Mai University (CMU) via the CMU Proactive Researcher project, Chiang Mai University [grant number: 572/2567]. This project was supported by the National Research Council of Thailand (NRCT) and Chiang Mai University [grant number: N42A670317]. The authors acknowledge the computational resource from Computational Simulation and Modeling Laboratory (CSML), Chiang Mai University. Numerical calculations were partially conducted at the Research Center for Computational Science, Institute for Molecular Science, National Institutes of Natural Sciences (project 23-IMS-C068 and 24-IMS-C066) and using MCRP-S at the Center for Computational Science, University of Tsukuba. This work was supported by MEXT as “Program for Promoting Researches on the Supercomputer Fugaku” (Data-Driven Research Methods Development and Materials Innovation Led by Computational Materials Science, JPMXP1020230327) and used computational resources of supercomputer Fugaku provided by the RIKEN Center for Computational Science (Project ID: hp230212 and hp240223) and the MEXT Program: Data Creation and Utilization-Type Material Research and Development Project Grant No. JPMXP1122714694. N.Y. was also supported by JSPS-KAKENHI 22H05089, 24K01434, 22H01873, and 24H00282. Molecular graphics were produced using Chimera.⁵⁶

REFERENCES

- (1) Barrow, S. J.; Kasera, S.; Rowland, M. J.; Del Barrio, J.; Scherman, O. A. Cucurbituril-Based Molecular Recognition. *Chem. Rev.* **2015**, *115* (2), 12320–12406.
- (2) Balaram, P.; William, L. Mock and Cucurbituril: The Resurrection of the Behrend Paper of 1905. *ACS Omega* **2024**, *9* (4), 4162–4165.
- (3) Chiangraeng, N.; Nakano, H.; Nimmanpipug, P.; Yoshida, N. Selective Molecular Recognition of Amino Acids and Their Derivatives by Cucurbiturils in Aqueous Solution: An MD/3D-RISM Study. *J. Mol. Liq.* **2023**, *386*, No. 122503.
- (4) Uzunova, V. D.; Cullinane, C.; Brix, K.; Nau, W. M.; Day, A. I. Toxicity of Cucurbit[7]Urils and Cucurbit[8]Urils: An Exploratory in Vitro and in Vivo Study. *Org. Biomol. Chem.* **2010**, *8* (9), 2037–2042.
- (5) Buczkowski, A.; Gorzkiewicz, M.; Stepniak, A.; Malinowska-Michalak, M.; Tokarz, P.; Urbaniak, P.; Ionov, M.; Klajnert-Maculewicz, B.; Palecz, B. Physicochemical and in Vitro Cytotoxicity Studies of Inclusion Complex between Gemcitabine and Cucurbit[7]-Urils. *Bioorg. Chem.* **2020**, *99*, No. 103843.
- (6) Zhikol, O. A.; Miasnikova, D. Y.; Vashchenko, O. V.; Pinchukova, N. A.; Zbruyev, O. I.; Shishkina, S. V.; Kyrychenko, A.; Chebanov, V. A. Host-Guest Complexation of (Pyridinyl)triazolylthio) Acetic Acid with Cucurbit[*n*]Urils (*n* = 6,7,8): Molecular Calculations and Thermogravimetric Analysis. *J. Mol. Struct.* **2023**, *1294*, No. 136532.
- (7) Chen, Y.; Huang, Z.; Zhao, H.; Xu, J. F.; Sun, Z.; Zhang, X. Supramolecular Chemotherapy: Cooperative Enhancement of Antitumor Activity by Combining Controlled Release of Oxaliplatin and Consuming of Spermine by Cucurbit[7]Urils. *ACS Appl. Mater. Interfaces* **2017**, *9* (10), 8602–8608.
- (8) Pashkina, E. A.; Grishina, L. V.; Aktanova, A. A.; Kozlov, V. A. Antitumor Activity of Supramolecular Complexes of Cucurbituril with Platinum(II) Compounds. *Inorg. Chim. Acta* **2021**, *522*, No. 120370.
- (9) Wheate, N. J.; Buck, D. P.; Day, A. I.; Collins, J. G. Cucurbit[*n*]Urils Binding of Platinum Anticancer Complexes. *Dalt. Trans.* **2006**, *3*, 451–458.
- (10) Buczkowski, A.; Tokarz, P.; Stepniak, A.; Lewkowski, J.; Rodacka, A.; Palecz, B. Spectroscopic and Calorimetric Studies of Interactions between Mitoxantrone and Cucurbituril Q7 in Aqueous Solutions. *J. Mol. Liq.* **2019**, *290*, No. 111190.
- (11) Buczkowski, A.; Tokarz, P.; Palecz, B. Thermodynamic Study of Ethanol Impact on Gemcitabine Binding to Cucurbit[7]Urils in Aqueous Solutions. *J. Chem. Thermodyn.* **2021**, *153*, No. 106317.
- (12) Buczkowski, A.; Stepniak, A.; Urbaniak, P.; Palecz, B. Calorimetric and Spectroscopic Investigations of Interactions between Cucurbituril Q7 and Gemcitabine in Aqueous Solutions. *J. Therm. Anal. Calorim.* **2018**, *134* (1), 595–607.
- (13) Wu, H. M.; Wang, S. L.; Li, X. X.; Ai, K. X. Fabrication of Gemcitabine and Mitoxantrone Loaded PLG/Mesoporous Silica Nanofibers: Investigation of In Vitro Drug Release and Anticancer Activity in Pancreatic Cancer Cells. *BioNanoScience* **2025**, *15*, 166.
- (14) Zhang, W.; Wang, Y.; Gu, M.; Mao, Z.; Guan, Y.; Wang, J.; Mao, W.; Yuan, W. E. Manganese Nanosheets Loaded with Selenium and Gemcitabine Activate the Tumor Microenvironment to Enhance Antitumor Immunity. *J. Colloid Interface Sci.* **2025**, *682*, 556–567.
- (15) Anderson, H.; Lund, B.; Bach, F.; Thatcher, N.; Walling, J.; Hansen, H. H. Single-Agent Activity of Weekly Gemcitabine in Advanced Non-Small-Cell Lung Cancer: A Phase II Study. *J. Clin. Oncol.* **1994**, *12* (9), 1821–1826.
- (16) Leijen, S.; Burgers, S. A.; Baas, P.; Pluim, D.; Tibben, M.; van Werkhoven, E.; Alessio, E.; Sava, G.; Beijnen, J. H.; Schellens, J. H. M. Phase I/II Study with Ruthenium Compound NAMI-A and Gemcitabine in Patients with Non-Small Cell Lung Cancer after First Line Therapy. *Invest. New Drugs* **2015**, *33* (1), 201–214.
- (17) Andreana, I.; Bincoletto, V.; Ricci, C.; Salaroglio, I. C.; Manzoli, M.; Zurletti, B.; Milone, J.; Rolando, B.; Del Favero, E.; Riganti, C.; Matricardi, P.; Stella, B.; Arpicco, S. Smart Hyaluronated Micelles to Enhance a Gemcitabine Prodrug Efficacy. *J. Drug Delivery Sci. Technol.* **2025**, *104*, No. 106518.
- (18) van der Heijden, M. S.; Sonpavde, G.; Powles, T.; Necchi, A.; Burotto, M.; Schenker, M.; Sade, J. P.; Bamias, A.; Beuzeboc, P.; Bedke, J.; Oldenburg, J.; Chatta, G.; Ürün, Y.; Ye, D.; He, Z.; Valderrama, B. P.; Ku, J. H.; Tomita, Y.; Filian, J.; Wang, L.; Purcea, D.; Patel, M. Y.; Nasroulah, F.; Galsky, M. D. Nivolumab plus Gemcitabine–Cisplatin in Advanced Urothelial Carcinoma. *N. Engl. J. Med.* **2023**, *389* (19), 1778–1789.
- (19) Moysan, E.; Bastiat, G.; Benoit, J. P. Gemcitabine versus Modified Gemcitabine: A Review of Several Promising Chemical Modifications. *Mol. Pharmaceutics* **2013**, *10* (2), 430–444.
- (20) Zou, L.; Braegelman, A. S.; Webber, M. J. Spatially Defined Drug Targeting by in Situ Host-Guest Chemistry in a Living Animal. *ACS Cent. Sci.* **2019**, *5* (6), 1035–1043.
- (21) Reddy, L.; Couvreur, P. Novel Approaches to Deliver Gemcitabine to Cancers. *Curr. Pharm. Des.* **2008**, *14* (11), 1124–1137.
- (22) Pan, G.; Mou, Q.; Ma, Y.; Ding, F.; Zhang, J.; Guo, Y.; Huang, X.; Li, Q.; Zhu, X.; Zhang, C. PH-Responsive and Gemcitabine-Containing DNA Nanogel to Facilitate the Chemodrug Delivery. *ACS Appl. Mater. Interfaces* **2019**, *11* (44), 41082–41090.
- (23) Dutta, B.; Shelar, S. B.; Barick, K. C.; Shetty, P.; Chakravarty, R.; Chakraborty, S.; Checker, S.; Sarma, H. D.; Hassan, P. A. Surface Engineered Fe₃O₄ Nanomagnets for PH-Responsive Delivery of Gemcitabine Hydrochloride and in Vivo Tracking by Radiolabeling. *Mater. Adv.* **2023**, *4* (1), 195–204.
- (24) Zang, W.; Gao, D.; Yu, M.; Long, M.; Zhang, Z.; Ji, T. Oral Delivery of Gemcitabine-Loaded Glycocholic Acid-Modified Micelles for Cancer Therapy. *ACS Nano* **2023**, *17* (18), 18074–18088.
- (25) Farrell, J. J.; Elsaleh, H.; Garcia, M.; Lai, R.; Ammar, A.; Regine, W. F.; Abrams, R.; Benson, A. B.; Macdonald, J.; Cass, C. E.; Dicker, A. P.; Mackey, J. R. Human Equilibrative Nucleoside Transporter 1 Levels

Predict Response to Gemcitabine in Patients with Pancreatic Cancer. *Gastroenterology* **2009**, *136* (1), 187–195.

(26) Diez-Fernández, R.; Vázquez-Sánchez, R.; López-Esteban, L.; Enrech-Frances, S.; Sánchez-Peña, A. M.; Díaz-Paniagua, L.; Soría-Tristán, M.; Martín Martínez, J. M.; Molina-García, T. Ethanol-Induced Symptoms in Patients Receiving Gemcitabine Diluted from a Concentrate for Solution for Infusion Containing Ethanol. *J. Oncol. Pharm. Pract.* **2018**, *24* (7), 511–516.

(27) Buczkowski, A. Thermodynamic Study of PH and Sodium Chloride Impact on Gemcitabine Binding to Cucurbit[7]Uril in Aqueous Solutions. *J. Mol. Liq.* **2022**, *345*, No. 117857.

(28) Venkataramanan, N. S.; Suvitha, A.; Sahara, R.; Kawazoe, Y. Unveiling the Gemcitabine Drug Complexation with Cucurbit[*n*]Urils (*n* = 6–8): A Computational Analysis. *Struct. Chem.* **2023**, *34* (5), 1869–1882.

(29) Chiangraeng, N.; Nakano, H.; Nimmanpipug, P.; Yoshida, N. Theoretical Analysis of the Role of Water in Ligand Binding to Cucurbit[*n*]Uril of Different Sizes. *J. Phys. Chem. B* **2023**, *127* (16), 3651–3662.

(30) Hirata, F. *Molecular Theory of Solvation*; Kluwer, Dordrecht: The Netherlands, 2003.

(31) Yoshida, N. Role of Solvation in Drug Design as Revealed by the Statistical Mechanics Integral Equation Theory of Liquids. *J. Chem. Inf. Model.* **2017**, *57* (11), 2646–2656.

(32) Imai, T. Molecular Theory of Partial Molar Volume and Its Applications to Biomolecular Systems. *Condens. Matter Phys.* **2007**, *10* (3), 343–361.

(33) Yoshida, N.; Hirata, F. A New Method to Determine Electrostatic Potential around a Macromolecule in Solution from Molecular Wave Functions. *J. Comput. Chem.* **2006**, *27* (4), 453–462.

(34) Yoshida, N.; Kiyota, Y.; Hirata, F. The Electronic-Structure Theory of a Large-Molecular System in Solution: Application to the Intercalation of Proflavine with Solvated DNA. *J. Mol. Liq.* **2011**, *159* (1), 83–92.

(35) Kovalenko, A.; Hirata, F. Self-Consistent Description of a Metal-Water Interface by the Kohn-Sham Density Functional Theory and the Three-Dimensional Reference Interaction Site Model. *J. Chem. Phys.* **1999**, *110* (20), 10095–10112.

(36) Sato, H.; Kovalenko, A.; Hirata, F. Self-Consistent Field, Ab Initio Molecular Orbital and Three-Dimensional Reference Interaction Site Model Study for Solvation Effect on Carbon Monoxide in Aqueous Solution. *J. Chem. Phys.* **2000**, *112* (21), 9463–9468.

(37) Schmidt, M. W.; Baldrige, K. K.; Boatz, J. A.; Elbert, S. T.; Gordon, M. S.; Jensen, J. H.; Koseki, S.; Matsunaga, N.; Nguyen, K. A.; Su, S.; Windus, T. L.; Dupuis, M.; Montgomery, J. A., Jr. General Atomic and Molecular Electronic Structure System. *J. Comput. Chem.* **1993**, *14* (11), 1347–1363.

(38) Perkyuns, J. S.; Montgomery Pettitt, B. A Dielectrically Consistent Interaction Site Theory for Solvent—Electrolyte Mixtures. *Chem. Phys. Lett.* **1992**, *190* (6), 626–630.

(39) Standards., U. S. B of. *Circular of the Bureau of Standards No. 19*, 6th ed.; National Bureau of Standards: Washington, D.C., 1924.

(40) Frisch, M. J.; Trucks, G. W.; Schlegel, H. B.; Scuseria, G. E.; Robb, M. A.; Cheeseman, J. R.; Scalmani, G.; Barone, V.; Petersson, G. A.; Nakatsuji, H.; Li, X.; Caricato, M.; Marenich, A. V.; Bloino, J.; Janesko, B. G.; Gomperts, R.; Mennucci, B.; Hratchian, H. P.; Ortiz, J. V.; Izmaylov, A. F.; Sonnenberg, J. L.; Williams-Young, D.; Ding, F.; Lipparini, F.; Egidi, F.; Goings, J.; Peng, B.; Petrone, A.; Henderson, T.; Ranasinghe, D.; Zakrzewski, V. G.; Gao, J.; Rega, N.; Zheng, G.; Liang, W.; Hada, M.; Ehara, M.; Toyota, K.; Fukuda, R.; Hasegawa, J.; Ishida, M.; Nakajima, T.; Honda, Y.; Kitao, O.; Nakai, H.; Vreven, T.; Throssell, K.; Montgomery, J. A., Jr.; Peralta, J. E.; Ogliaro, F.; Bearpark, M. J.; Heyd, J. J.; Brothers, E. N.; Kudin, K. N.; Staroverov, V. N.; Keith, T. A.; Kobayashi, R.; Normand, J.; Raghavachari, K.; Rendell, A. P.; Burant, J. C.; Iyengar, S. S.; Tomasi, J.; Cossi, M.; Millam, J. M.; Klene, M.; Adamo, C.; Cammi, R.; Ochterski, J. W.; Martin, R. L.; Morokuma, K.; Farkas, O.; Foresman, J. B.; Fox, D. J. *Gaussian 16, Rev. C.01*, Gaussian, Inc.: Wallingford CT, 2019.

(41) Kovalenko, A.; Hirata, F. Potentials of Mean Force of Simple Ions in Ambient Aqueous Solution. II. Solvation Structure from the Three-Dimensional Reference Interaction Site Model Approach, and Comparison with Simulations. *J. Chem. Phys.* **2000**, *112* (23), 10403–10417.

(42) Wang, J.; Wang, W.; Kollman, P. A.; Case, D. A. Automatic Atom Type and Bond Type Perception in Molecular Mechanical Calculations. *J. Mol. Graph. Model.* **2006**, *25* (2), 247–260.

(43) Martínez, L.; Andrade, R.; Birgin, E. G.; Martínez, J. M. PACKMOL: A Package for Building Initial Configurations for Molecular Dynamics Simulations. *J. Comput. Chem.* **2009**, *30* (13), 2157–2164.

(44) Salomon-Ferrer, R.; Götz, A. W.; Poole, D.; Le Grand, S.; Walker, R. C. Routine Microsecond Molecular Dynamics Simulations with AMBER on GPUs. 2. Explicit Solvent Particle Mesh Ewald. *J. Chem. Theory Comput.* **2013**, *9* (9), 3878–3888.

(45) Götz, A. W.; Williamson, M. J.; Xu, D.; Poole, D.; Le Grand, S.; Walker, R. C. Routine Microsecond Molecular Dynamics Simulations with AMBER on GPUs. 1. Generalized Born. *J. Chem. Theory Comput.* **2012**, *8* (5), 1542–1555.

(46) Le Grand, S.; Götz, A. W.; Walker, R. C. SPFP: Speed without Compromise - A Mixed Precision Model for GPU Accelerated Molecular Dynamics Simulations. *Comput. Phys. Commun.* **2013**, *184* (2), 374–380.

(47) Andersen, H. C. Rattle: A “Velocity” Version of the Shake Algorithm for Molecular Dynamics Calculations. *J. Comput. Phys.* **1983**, *52* (1), 24–34.

(48) Roe, D. R.; Cheatham, T. E. PTRAJ and CPPTRAJ: Software for Processing and Analysis of Molecular Dynamics Trajectory Data. *J. Chem. Theory Comput.* **2013**, *9* (7), 3084–3095.

(49) Maruyama, Y.; Yoshida, N. RISMCal: A Software Package to Perform Fast RISM/3D-RISM Calculations. *J. Comput. Chem.* **2024**, *45* (17), 1470–1482.

(50) Yoshida, N. The Reference Interaction Site Model Integrated Calculator (RISMCal) Program Package for Nano- and Biomaterials Design. *IOP Conf. Ser. Mater. Sci. Eng.* **2020**, *773* (1), No. 012062.

(51) Singer, S. J.; Chandler, D. Free Energy Functions in the Extended RISM Approximation. *Mol. Phys.* **1985**, *55* (3), 621–625.

(52) Kovalenko, A.; Hirata, F. Potential of Mean Force between Two Molecular Ions in a Polar Molecular Solvent: A Study by the Three-Dimensional Reference Interaction Site Model. *J. Phys. Chem. B* **1999**, *103* (37), 7942–7957.

(53) Imai, T.; Harano, Y.; Kinoshita, M.; Kovalenko, A.; Hirata, F. A Theoretical Analysis on Hydration Thermodynamics of Proteins. *J. Chem. Phys.* **2006**, *125* (2), No. 024911.

(54) Tanimoto, S.; Yoshida, N.; Yamaguchi, T.; Ten-No, S. L.; Nakano, H. Effect of Molecular Orientational Correlations on Solvation Free Energy Computed by Reference Interaction Site Model Theory. *J. Chem. Inf. Model.* **2019**, *59* (9), 3770–3781.

(55) Sergievskiy, V.; Jeanmairet, G.; Levesque, M.; Borgis, D. Solvation Free-Energy Pressure Corrections in the Three Dimensional Reference Interaction Site Model. *J. Chem. Phys.* **2015**, *143* (18), No. 184116.

(56) Pettersen, E. F.; Goddard, T. D.; Huang, C. C.; Couch, G. S.; Greenblatt, D. M.; Meng, E. C.; Ferrin, T. E. UCSF Chimera - a Visualization System for Exploratory Research and Analysis. *J. Comput. Chem.* **2004**, *25* (13), 1605–1612.